Canadian Conference - Pacific Conference on Earthquake Engineering 2023

Vancouver, British Columbia

June 25th – June 30th, 2023

Considering Corrosion Conditioning In Seismic Evaluation Of Corroded Reinforced Concrete Columns

Farah Dameh[1*], Nicolas El-Joukadar[2*] and Stavroula Pantazopoulou[3]

[1]PhD Student, Department of Civil Engineering, York University, Toronto, ON, CA
[2]Senior Project Coordinator, EllisDon, Toronto, ON, Canada
[3]Professor, Department of Civil Engineering, York University, Toronto, ON, CA
[*]fardam96@yorku.ca, njoukhadar9@gmail.com (Corresponding Author)

ABSTRACT

Corrosion impacts the condition and properties of reinforced concrete members leading to loss of lateral load resistance and deformation capacity. It has been shown through experiment and field evidence that corrosion may degrade a seismically well-designed ductile component to behaving as a poorly-detailed, brittle one. Corrosion reduces the strength in many different ways: first, by means of reducing the stirrup diameter, thereby deteriorating the shear strength, the confinement effectiveness, stability of longitudinal bars in compression, and the development capacity in lap splices. Also, the accumulation of iron rust imposes pressure on the concrete covers causing them to eventually split and delaminate. This in turn reduces the bond strength of lap splices and anchorages. Carbonation-induced corrosion depletes the microstructure of concrete from calcium minerals, causing embrittlement of concrete – it also affects the chemical structure of the reinforcement causing reduced yield strength and deformation capacity at rupture. As corroded concrete members can be found in existing construction in several regions of moderate and high seismicity around the world, modelling of such cases becomes crucial for the purpose of seismic assessment of affected structures. In the present study, detailed finite element models for corroded columns were developed using nonlinear modeling by introducing attenuated properties of yield and ultimate strength and deformation capacity of reinforcement, which were derived from an updated database of material tests on corroded bar samples. The modelled corroded columns also accounted for the reduction of bond strength and cover due to rust expansion and stirrup section loss and two types of detailing, i.e., continuous anchored columns and lap splices. The modelling approach was calibrated against well-known experiments for the purpose of model validation under reversed cyclic displacement histories simulating earthquake effects. It was concluded that the deformation capacities of corroded columns were the most affected by corrosion. Additionally, the columns with lapped splices were more affected by the corrosion relative to columns with full anchorage. A simplified procedure for seismic assessment of members was also calibrated with the numerical results, introducing attenuation factors that consider the extent of corrosion, in order to reduce the yield and ultimate strengths and drift capacity of corroded columns from their reference nominal uncorroded values.

Keywords: Seismic Assessment, Corrosion, Durability, Finite Element Analysis, Numerical Study.

INTRODUCTION

The seismic assessment of reinforced concrete structures follows the performance criteria provided in ASCE SEI 41/17 [1]. These assessment procedures are used to compare seismic demand and capacity in order to predict future seismic damage. Despite the fact that many existing structures have been exposed to preexisting damage prior to its exposure to seismic demands (such as high risk of reinforcement corrosion and cover concrete strength degradation), no explicit procedures have been provided in assessment codes to predict the capacity of such components. The major effects of corrosion on the response of RC components is predicted though its impact on structural material properties. The process of carbonation or the gradual concentration of chloride ions on the bar surface transported by moisture through concrete's capillary pores, causes an effective decrease of the pH value, which triggers the formation of oxygen-iron compounds. The amount of time needed to cause the decrease in the pH value is called the "initiation period"[2]. Corrosion byproducts (various oxides) are two to ten times the volume of steel [3]. Additionally, the increased amount of newly formed rust causes radial bursting pressure around the reinforcement, which eventually leads to radial cracking of the concrete cover along the bar length. Thus, reduced stiffness and strength is another attribute of corroded reinforced concrete members. The present study focuses on finite element modelling of corroded reinforced concrete columns using the implication of these processes, which is reflected in the deterioration of material strength of corroded members.

OBJECTIVES

The objective of this study includes: (a) developing quantitative models that may be used for simulation of the mechanical properties of corroded columns. The reduced properties of ultimate/ yield strength, strain rupture of corroded reinforcement were derived from an updated database of material tests on corroded reinforcement. These reduced mechanical properties were formulated with reference to mass loss of reinforcement. (b) Validation of the developed formulation of reduced yield, ultimate and strain rupture through adjustments of material properties in advanced finite element models (using ATENA GiD 15.0.2 [4]) by reproducing the performance of laboratory tested columns with corroded reinforcement (Goksu & Ilki [5]). (c) Conduct a numerical and parametric investigation of corroded columns with different reinforcement detailing (lap splice and continuous reinforcement) and mass loss amount.

METHODOLOGY

Detailed finite element models are developed for columns considering the reduced strength and strain of corroded reinforcement to validate the proposed approach.

Material Models of Cracked Concrete Cover, Reinforcement and Bond in Corroded Columns

A database of yield strength, ultimate strength, and strain rupture of 300 experimentally tested corroded reinforcement was assembled by El-Joukhadar et al. [6]. Figures 1(a), (b) and (c) plot the assembled data of the residual ultimate strength, residual yield strength and residual strain rupture of corroded bars against the increasing reinforcement mass loss, x. The mass loss of reinforced bars is the primary parameter found in literature that quantifies the amount of corrosion. Equation (1) may be used to calculate the reduced bar diameter, D_{cor} , after corrosion, given the value of x (in percent). M_0 and D_0 are the mass per unit length and diameter of the un-corroded bar(s), and M_{cor} is the residual mass per unit length of the corroded bar(s).

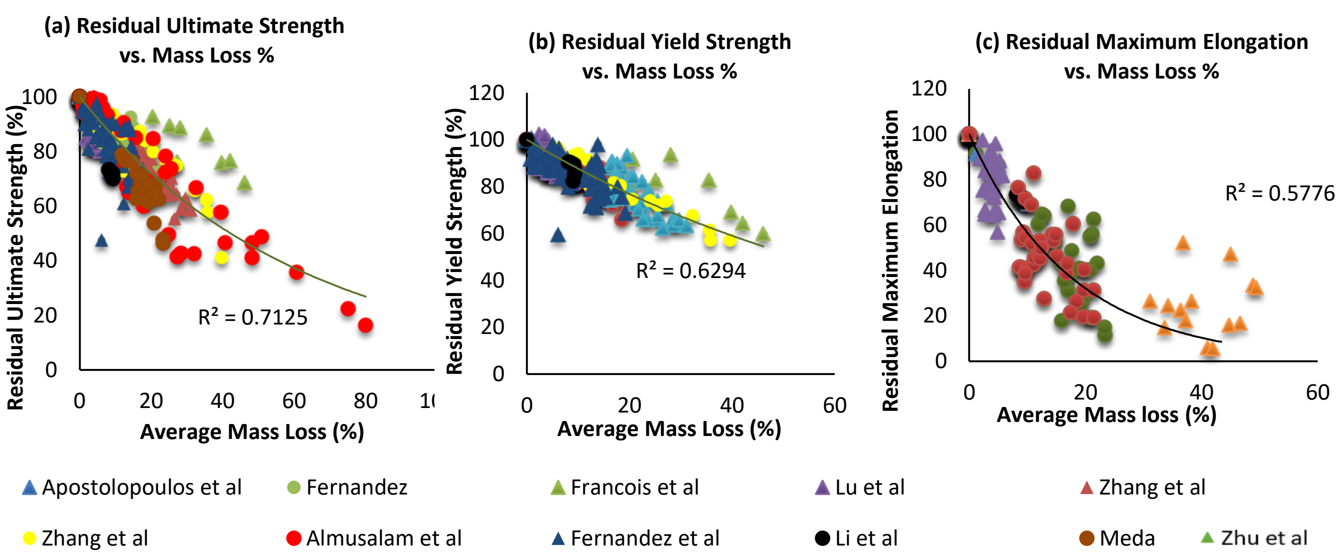

Figure 1.Corroded steel tests: (a) residual ultimate strength of corroded reinforcement Vs. mass loss, x, (b) residual yield strength of corroded reinforcement Vs. mass loss, x, (c) residual maximum elongation of corroded reinforcement Vs. mass loss, x.[11]

$$x = \frac{M_0 - M_{cor}}{M_0} \cdot 100 = \left(1 - \left(\frac{D_{Cor}}{D_0}\right)^2\right) \cdot 100 \rightarrow D_{cor} = D_o \cdot \sqrt{1 - \frac{x}{100}} \quad (1)$$

The data gathered in Fig. 1 (a), (b) and (c) were divided into two groups based on the corrosion type: 1) tests conducted on naturally corroded bars (marked with triangles). 2) galvanostatic or potentiostatic corrosion (by using impressed current or voltage- marked by circles). The material properties are affected in the same way for both corrosion types with higher strength reduction in the naturally corroded ones. Equations (2-4) obtained through regression analysis represent the residual yield strength, $f_{y,res}$, ultimate strength, $f_{u,res}$ and ultimate elongation, $\varepsilon_{u,res}$, of corroded bars with increasing amount of average steel mass loss ratio, x.

$$\boldsymbol{f_{y,res}} = \boldsymbol{f_y} \cdot e^{-0.013x} \tag{2}$$

$$\boldsymbol{f_{u,res}} = \boldsymbol{f_u} \cdot \mathrm{e}^{-0.016x} \tag{3}$$

$$\varepsilon_{u,res} = \varepsilon_u \cdot e^{-0.057x} \tag{4}$$

In Eqns. (2-4), parameters f_y, f_u and ε_u represent the reference uncorroded values for yield, ultimate strength and ultimate strain capacity respectively. Table 1 depicts the estimated residual bond strength of corroded reinforcement as per *fib*-Model Code 2010 [7], which takes into account the cases of presence and absence of stirrups using the corrosion penetration parameter C_p as shown in Eq. (5):

$$C_p = (D_0 - D_{cor})/2 = 0.5 \cdot D_0 \left(1 - \sqrt{1 - \frac{x}{100}}\right) \tag{5}$$

Table 1. Magnitude of Bond Strength for Corroded Members from fib 2010 [7]

Corrosion Penetration mm. (in×10³)	***Equivalent Surface Crack mm. (in×10³)***	***Confinement***	***Residual Bond Strength (% of f_b). Bar Type:***	
			Ribbed	***Plain***
0.05 (0.197)	*0.2-0.4 (0.79-1.57)*	***No stirrups***	*50-70*	*70-90*
0.1 (0.394)	*0.4-0.8 (1.57-3.1)*		*40-50*	*50-60*
0.25 (0.98)	*1.0-2.0 (39-79)*		*25-40*	*30-40*
0.05 (0.197)	*0.2-0.4 (0.79-1.57)*	***with Stirrups***	*95-100*	*95-100*
0.1 (0.394)	*0.4-0.8 (1.57-31)*		*70-80*	*95-100*
0.25 (0.98)	*1.0-2.0 (39-79)*		*60-75*	*90-100*

The increase of the volume of the corrosion by-products results in reduction of cover strength through longitudinal cracking along the corroded bar. Thus, the concrete cover strength ought to be reduced to yield more accurate assessments. Equation 6, developed by Coronelli and Gambarova[8], was used to model the reduced strength of concrete in corroded columns. The decrease in the tensile strength of the concrete that occurs due to transverse splitting ε_1 was modelled from Coronelli and Gambarova [8], from the modified diagonal compression field theory [9].

$$\boldsymbol{f_{c,res}} = \frac{f'_c}{1+0.1\frac{\varepsilon_1}{\varepsilon_{c0}}}\ ; \quad and,\ E_{c,res} = E_c \cdot \left(\boldsymbol{f_{c,res}}/\boldsymbol{f'_c}\right) \tag{6}$$

In Eq. (6), f'_c is the concrete's compressive strength, ε_{co} is the strain at peak compressive strength (=0.002), and ε_1 is the average tensile strain. It represents a smeared measure of splitting crack widths of the cover. Therefore, ε_1 is obtained from Eq. (7):

$$\varepsilon_1 = N_{cb} \cdot \left[\pi \cdot (\alpha_{rs} - 1) \cdot 2C_p\right]/b \tag{7}$$

Parameter N_{cb} represents the number of bars present in the cross-section's compression zone, b is the width of the cross-section and α_{rs} is the volume ratio of the oxides with respect to the parent metal.

Validation of Proposed Approach Using Finite Element Analysis

Columns tested by Goksu & Ilki[5] were scaled models of structural components (at a scale of 1:2). The columns' section and detailing is shown in Fig 2. The length of the shear span L_s was 1.2m and a cross-section was 200 mm width by 300 mm total depth. With an aspect ratio of 1:4, the aim was to obtain columns that fail in flexure. The column's longitudinal reinforcement consisted of 4Φ14 reinforcement with a lap length of 40Φ = 560mm. The total longitudinal reinforcement ratio was1.6%. Column transverse reinforcement consisted of Φ8 bars spaced at 100mm, with an unsupported bar aspect ratio equal to s/Φ=100/14=7. The applied axial load was 20% of the columns' axial capacity which was equivalent to 282 KN. The modelled columns were NS-X00, NS-X09, NS-X16 and NS-X22. The numeral following the letter X represents the fraction of mass loss of reinforcement after corrosion (term NS corresponds to Normal Strength concrete).

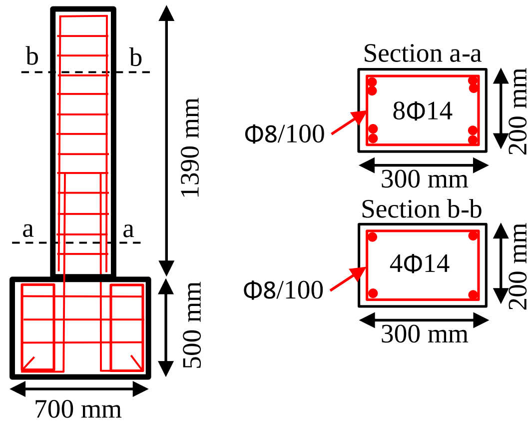

Fig. 2- Column detailing of Goksu and Ilki's experimental program [5][11]

The concrete material used in the columns' analytical model was "3D Nonlinear Cementitious2"[4]. The nonlinearity is expressed through the equivalent uniaxial strain ε^{eq}. The equivalent uniaxial strain is defined as the strain that is produced by the stress σ_{ci} in a uniaxial test with the modulus E_{ci} in the direction i ($\varepsilon^{eq} = \sigma_{ci}/E_{ci}$). For material properties: concrete compressive strength (f_c') was 25 MPa, the tensile strength (f_t) was taken equal to 2.5 MPa, Modulus of Elasticity ($E_c=4500\sqrt{f_c'}$) was equal to 22,500 MPa. The concrete fracture energy, G_F, was set equal to 130 N/m, and was determined based on the Model Code 2010 expression: $G_F= 73\cdot(f'_c)^{0.18}$. A rotated crack model was used, where the axis of the principal stress and principal strain coincide throughout loading and crack formation in the model, abandoning the development of shear strains along the crack plane. Concrete cover cracking was accounted for by reducing the compressive and tensile strengths of the concrete cover material; the compressive strength was reduced according to Eq (6) and the tensile strength was assumed to be entirely lost (i.e., neglected). Reinforcing bars were modelled as truss elements using the "Reinforcement" option, with a *bilinear-with-hardening type* of uniaxial stress-strain behavior with a steel modulus E_s equal to 200,000 MPa. Reinforcement mechanical properties are shown in Table 2.

Table 2. Material Properties Used to Model the Corroded Columns of Goksu and Ilki's [5] Using the Proposed Method [11]

Column ID		NS-X0	NS-X9	NS-X16	NS-X22
Mass loss (%)		0	9	16	22
Yield Strength f_y, MPa	Longitudinal	460	409	374	346
	Stirrups	486	432	395	365
Ultimate Strength f_u MPa	Longitudinal	652	565	505	459
	Stirrups	681	590	527	479
Max. strain ε_u	Longitudinal	0.116	0.071	0.049	0.035
	Stirrups	0.134	0.083	0.057	0.041
Concrete Cover Comp. Strength f_c, (MPa)		25	6.73	4.22	3.17
Resid. bond strength Normalized f_b		1.0	0.72	0.5	0.35

Adjustments were made on the reference model to represent columns with corroded reinforcement based on Eqs (2-4) with reference to the uncorded column case NS-X00. The bar diameters for both ties and longitudinal reinforcement were not decreased. This assumption was made based on the reduction in the strength following Eqs. (2-4). The Menegotto-Pinto model [10] with a Bauschinger R value = 7, C_1 value = 5000 and C_2 value = 20 using Eqs (8).

$$\boldsymbol{\sigma} = (\boldsymbol{\sigma_o} - \boldsymbol{\sigma_r})\boldsymbol{\sigma}^* + \boldsymbol{\sigma_r} \;; \quad \boldsymbol{\sigma}^* = b\varepsilon^* + \frac{(1-b)\varepsilon^*}{\left(1+\varepsilon^{*R}\right)^{\frac{1}{R}}}; \quad \varepsilon^* = \frac{\varepsilon-\varepsilon_r}{\varepsilon_o-\varepsilon_r}; \quad R = R_o - \frac{C_1\xi}{C_2+\xi} \tag{8}$$

In the above model, C_1 , C_2 and R are defined by the user. The subscript ($_o$) of strain (ε_o) and stress (σ_o) are the starting point of the hysteretic branch, while ($_r$) of strain (ε_r) and stress (σ_r) are the end point of the hysteretic branch. Strain ε corresponds to the bar stress σ. The bond stress-slip relationshsip assigned to the reinforcement is shown in Fig. 3 (a). As per Model Code 2010, the displacemnet at the onset of post peak S_3, was assumed equal to half the distance between successive ribs. As rib location is unaffected by corrosion the same values were used for S_3 for both corroded and un-corroded models. No plateau was considered at peak strength because splitting response was assumed. Therefore, the slip corresponding to the splitting strength S_1, coincided with the slip S_2 that corresponds to the onset of post-peak degradation of bond ($S_1 = S_2$). Interpolation of values of slip based on the uncorroeded splitting values was made to get the value of S_1 from Model code (2010). Figure 3 (b) depicts the bar with memory bond material [4] that was used to model the bond in ATENA GiD. When the direction of the bond reverses due to the reverses in loading direction, if loading exceeds the peak bond slip, the bond is then set equal to the residual bond strength. The residual bond strength in this study is taken as 0.4 of the maximum bond strength.

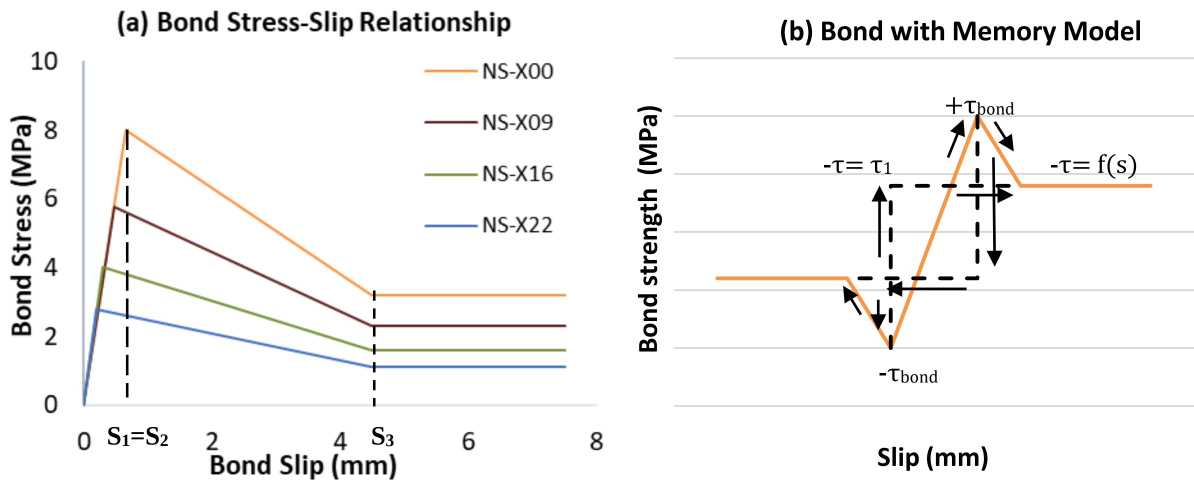

Figure 3. Bond properties: (a) bond stress-slip relationship in the models of Goksu and Ilki's [5] columns (b) bond cylic material properties[4,11]

The columns were modelled as a lateral swaying cantilever. Fixed surface at the bottom was applied and the top undergoes a relative displacement. Due to symmetry, only half of the cross section was modelled (i.e. *x-z* is the plane of symmetry, at $y=0$), with the condition that $u_y(x,0,z)=0$. Two plates with a thickness of 100 mm were used at the front and the back sides to apply lateral displacement at the centroid *(-0.1m, 0.0 m, 1.2m)*. The plate elements were assigned with "3D Elastic Isotropic" steel material [3].

Figure 4 depicts the resistance curves from the finite element analysis compared with the experimental results of Goksu & Ilki [5]. The graphs depict the lateral resistances against the displacement at the tip of the column. To eliminate the contribution of P – Delta effects the lateral resistance load was corrected according to Eqs. 9.

$$\boldsymbol{V_{res}} = \frac{M}{L_s} + \boldsymbol{P} \cdot \boldsymbol{\theta} \tag{9}$$

The product $P{\cdot}\theta$ was added to all lateral resistance values from the finite element analysis to correct for the P-Δ effects that the manner of load application introduced in the analysis which did not occur in the tests due to the use of prestressing rods for axial compression of the columns; in fact the experimental test setup in Goksu [4], has an additional component on account of the rotation of the cap beam on which the rods were bearing against. Therefore, the lateral resistance values for Goksu's [4] experiment were corrected according with Eq. 10.

$$\boldsymbol{V_{res}} = \boldsymbol{V_{exp}} + \boldsymbol{P} \cdot \theta \cdot \cos \boldsymbol{\theta_{tip}} - \boldsymbol{P} \cdot \sin \boldsymbol{\theta_{tip}}\ ; \quad \text{where,}\ \ \boldsymbol{\theta_{tip}} = 1.2 \cdot \boldsymbol{\theta} \tag{10}$$

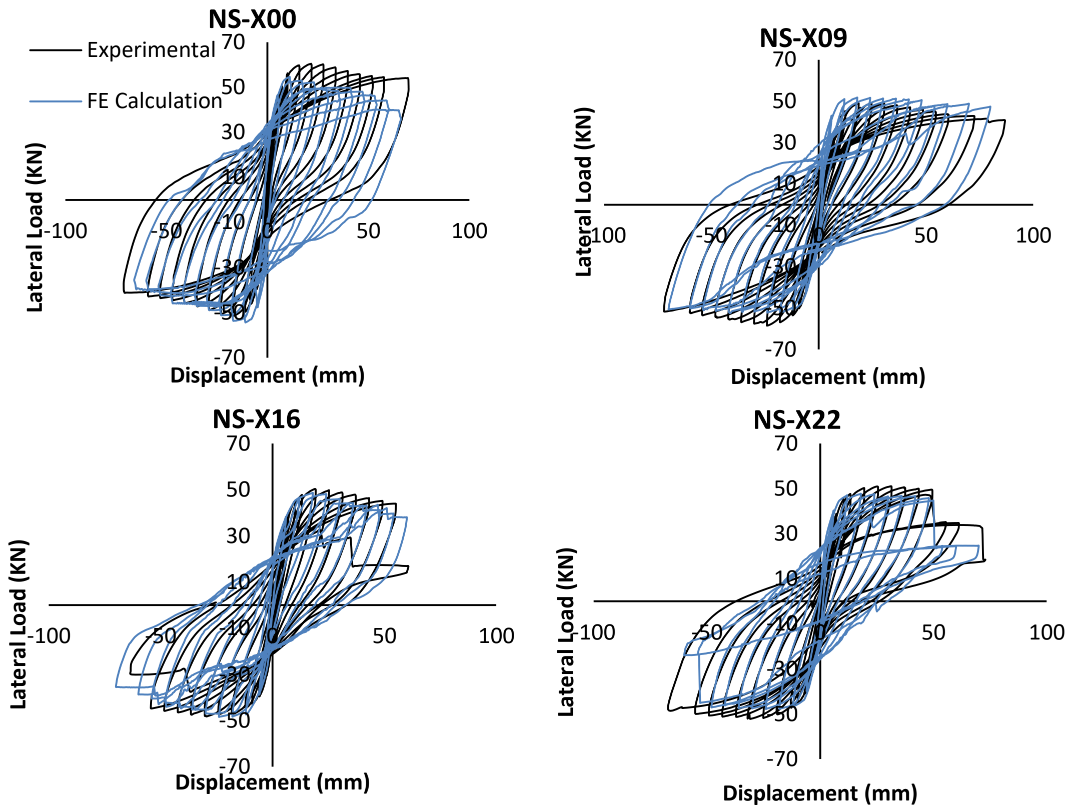

Figure 4. Response of finite element analysis of corroded columns of Goksu and Ilki's [5,11]

The response of the analytical columns were successful in replicating the response of the experimentally tested columns of Goksu & Ilki [4]. Minor differences between the experimental and numerical columns were found (for example in specimen NS-X00, it is noted that the model showed a symmetric response having a maximum load of about 50kN in both directions while the tested column did not). This behavior is common in tested columns, the non-symmetry owing to several factors; a main reason is that the damage towards one direction of sway, resets the geometry of the test setup in terms that are not found in the model (e.g. damage in the anchorages). Other factors that may contribute to the non- symmetry in the resistance curve of a tested column include: column fabrication, testing setup and hardware compliances. Generally, the columns successfully replicated the behavior of the columns, which validates the proposed approach for modelling material properties of corroded columns. In addition, the model successfully replicated the bond-failure in column NS-22 at a displacement level of 50mm.

Figure 5 depicts the crack pattern and stresses of columns NS-X00, NS-X09, NS-X16 and NS-X22 at a drift ratio of 4.5%. Figure 6 depicts the strains along the longitudinal reinforcement at maximum displacement. From Fig. 6 and 7 bond splitting and bar buckling is evident. The results from the finite element analysis provide sufficient evidence for model validation.

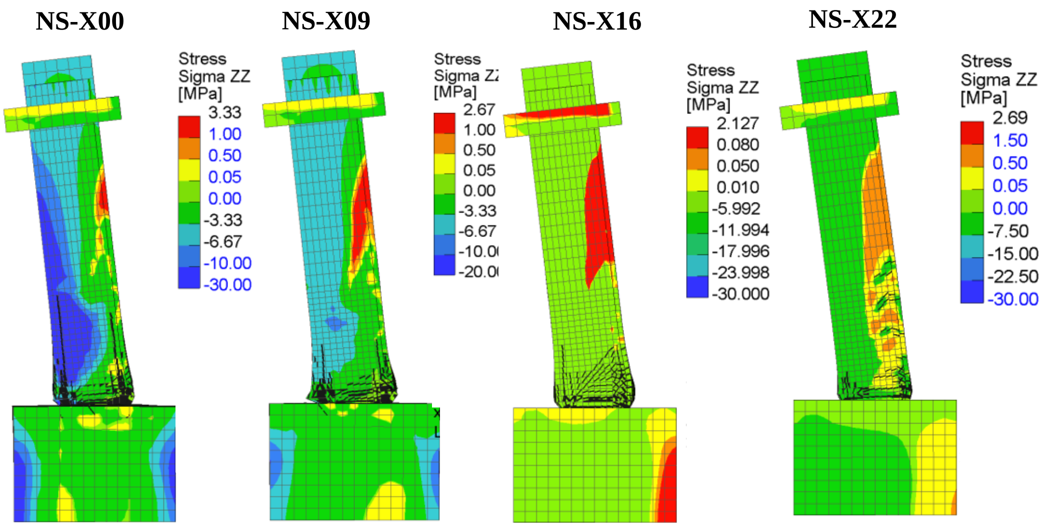

Figure 5. Crack pattern, stress distribution and failure modes of FEA [11]

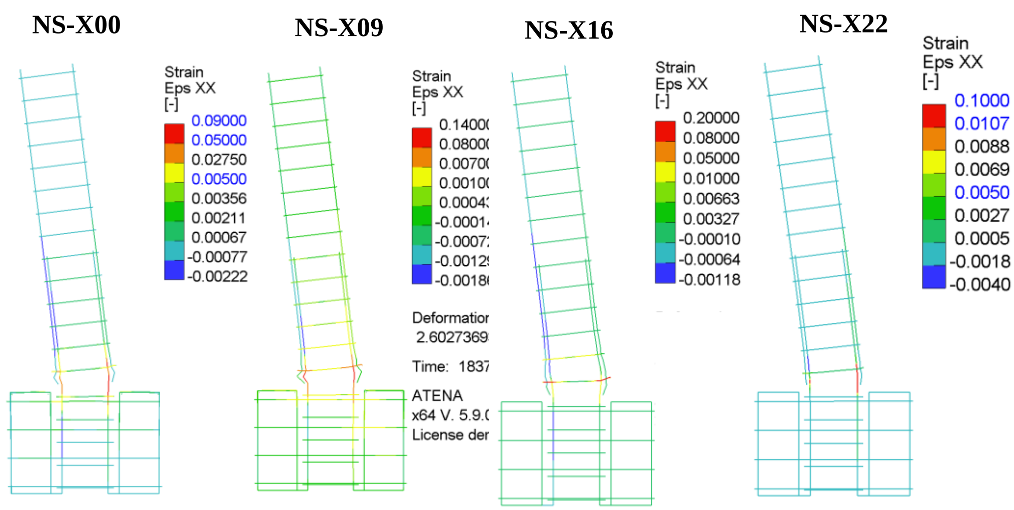

Figure 6. Strain in longitudinal reinforcement from FEA [11]

Numerical Investigation

The modeling procedure is used next in order to explore the parametric sensitivity of the problem. The columns used towards this goal represent pre-1970s design practices such as the use of short lap splices at the critical region, poor concrete material strength and sparse stirrup spacing. The variables of the study included: the degree of corrosion in terms of steel mass loss (0, 10% and 20%), reinforcement detailing including lap splices at the critical section and well anchored continuous reinforcement extending into the column foundation. The case identification code begins with A or L (for anchored or lap spliced longitudinal reinforcement), followed with the mass loss percentage. The column detailing is shown in Fig. 7. The columns had a cross section of 300 mm and a shear span of 1.65 m with 4-15M bars and 8mm diameter transverse reinforcement spaced at s=d=250mm. The length of the lap splices l_p was taken as $24\ D_b$ = 384mm. The mechanical properties of corroded reinforcement and concrete cover (following the proposed approach in this study) are shown in Table 3. Reference concrete compressive strength for corroded columns was taken as f'_c=25 MPa.

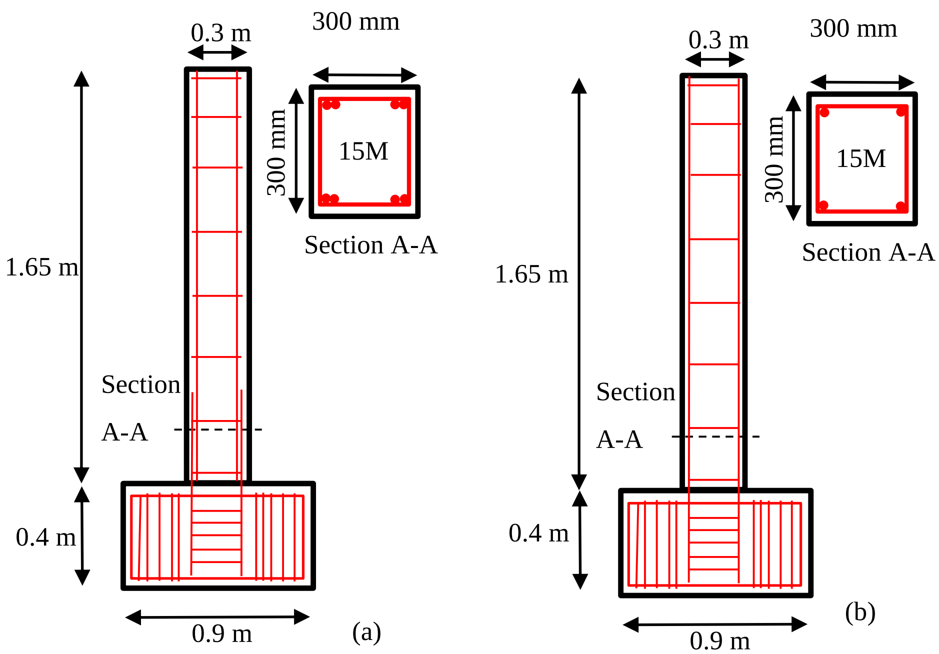

Figure 7. Detailing of columns for numerical investigation: (a) lap-spliced column, (b) anchored column[11]

Table 3. Calculated Residual Material Properties used in Column Models. **.** *[11]*

		Anchored Columns (A)			**Lap-Spliced Columns (L)**		
Mass loss		0%	10%	20%	0%	10%	20%
Column ID		A-0	A-10	A-20	L-0	L-10	L-20
Yield Strength (f_y) MPa	**Longitudinal**	420	369	324	420	369	324
	Stirrups	300	263	231	300	263	231
Ultimate Strength (f_u) MPa	**Longitudinal**	550	469	399	550	469	399
	Stirrups	380	324	276	380	324	276
Strain Rupture (ε_u)	**Longitudinal**	0.2	0.117	0.068	0.2	0.117	0.068
	Stirrups	0.2	0.117	0.068	0.2	0.117	0.068
Concrete Cover compressive strength (f_c) MPa		25	6.21	3.46	25	6.21	3.46

Numerical Results

Plots in Fig. 8 depict the hysteresis loops produced from the finite element analysis of the proposed columns on the left, while the right side plots are the normalized lateral resistance vs. the displacement envelopes. Un-corroded columns with anchored longitudinal reinforcement present a 10% higher lateral resistance compared to the un-corroded lap spliced column with equal amount of lateral strength at higher deformation levels. With a 10% mass loss, the strength reduces to 10% and 25% for the anchored and the lap splice cases respectively. Additionally, a 30% reduction in the deformation capacity was observed for columns with 10% mass loss as depicted in Fig. 8 (b). When increasing the bar mass loss to 20% the reduction in strength relative to the un-corroded columns increased to 20% and 40% for the cases of columns with anchored and lapped spliced reinforcement, respectively. Moreover, the ultimate deformation capacity was reduced by 45%. Table 4 provides an overview of the maximum lateral resistance for each case presented in Fig. 8.

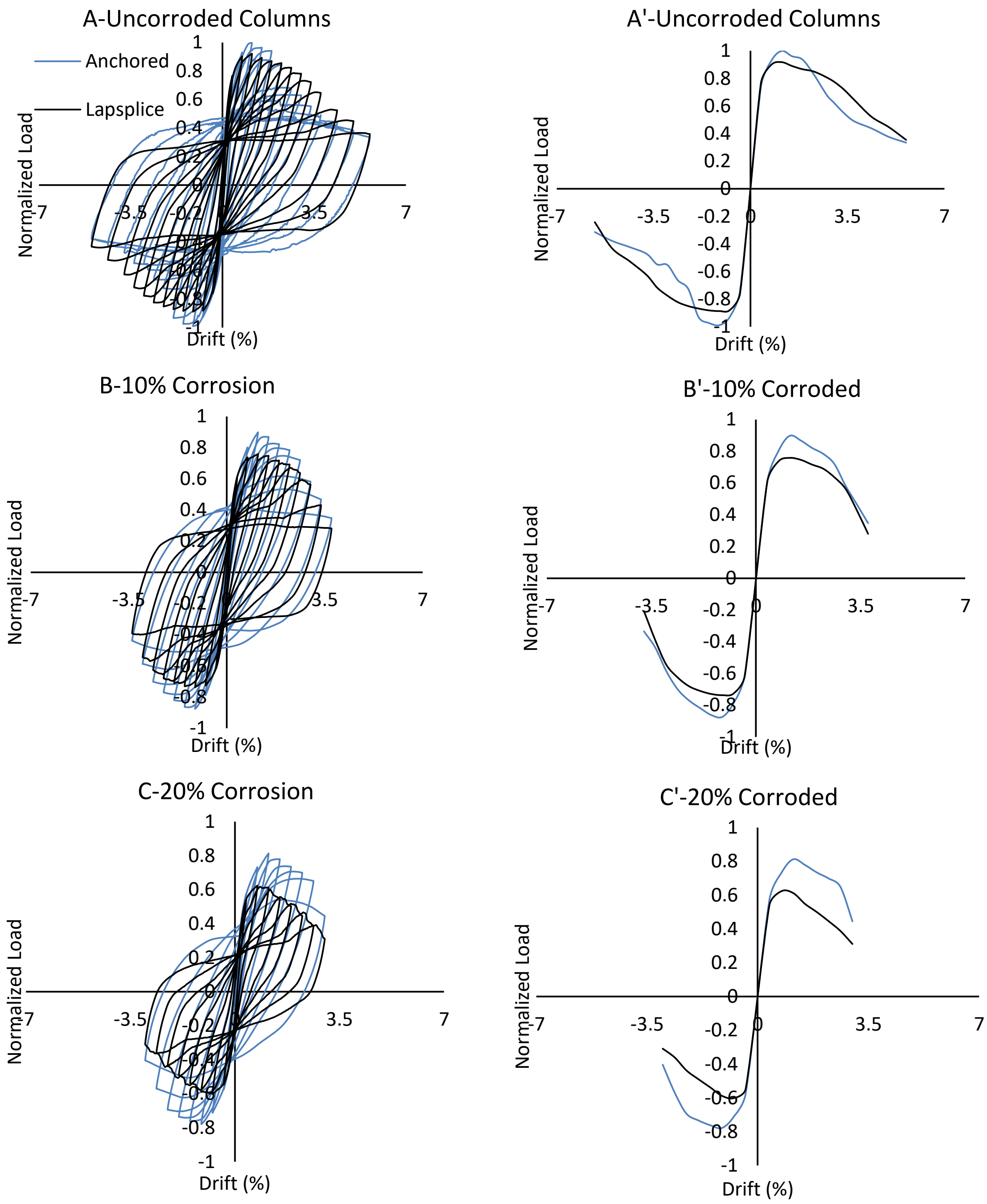

Figure 8. Hysteretic response and normalized envelopes of columns from the numerical study[11]

Table 4. Base Shear for Columns in the Numerical Investigation [11]

	Anchored Columns			**Lap-Spliced Columns**		
Mass loss	**0%**	**10%**	**20%**	**0%**	**10%**	**20%**
Column ID	**A-0**	**A-10**	**A-20**	**L-0**	**L-10**	**L-20**
Base Shear (kN)	69.5	59.4	54.3	61.2	51.9	42.1

The presented study provides basics for establishing required factors for attenuation of backbone cures for assessment of corroded columns specified by ASCE/SEI 41 (2017) as shown in Fig. 9. The ASCE Multipliers for the reduced back backbone curves are shown in Eq. 11, 12 and 13 [12] . Equation 11 depicts the reduction in elastic stiffness ($r_{k,1}$, $r_{k,1}$), Eq. 12 depicts the reduction in the peak strength ($r_{v,1}$, $r_{v,2}$), while Eq. 13 depicts the ultimate deformation capacity of the columns. The group is divided into two parts. Groups with Subscript ($_1$) which are columns with the axial load ratio of $0 \leq \nu \leq 20\%$, whereas the second group has a subscript ($_2$) and they refer to columns with an axial load ratio of $20\% \leq \nu \leq 40\%$.

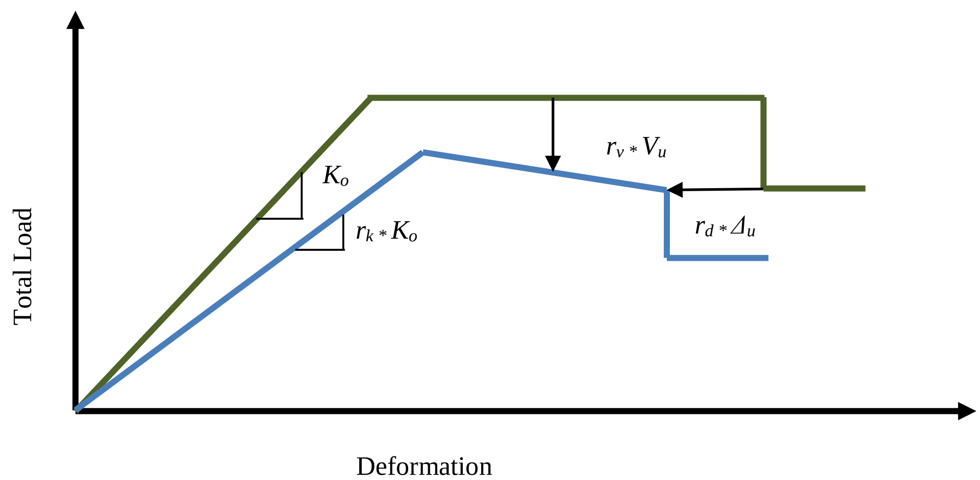

Figure 9. Resistance curve of corroded and uncorroded reinforced concrete members [11]

$$r_{k,1} = 1 - \frac{1.29 \cdot x}{100};\ r_{k,2} = 1 - \frac{1.07 \cdot x}{100} \tag{11}$$

$$r_{v,1} = \frac{V_{cor,1}}{V_{u,1}} = 1 - \frac{0.5 \cdot \theta \cdot x}{100};\ r_{v,2} = \frac{V_{cor,2}}{V_{u,2}} = 1 - \frac{0.8 \cdot \theta \cdot x}{100} \tag{12}$$

$$r_{d,1} = \frac{\Delta_{u,cor,1}}{\Delta_{u,0,1}} = 1 - \frac{2.2x}{100};\ r_{d,2} = \frac{\Delta_{u,cor,1}}{\Delta_{u,0,1}} = 1 - \frac{2.75x}{100} \tag{13}$$

The parameters in Eq. 11,12 and 13 are as follows: x is the loss of mass of steel, $\Delta_{u,cor,1}$ is the residual displacement capacity of corroded members, $\Delta_{u,0,1}$ is the displacement capacity of identical uncorroded member, $V_{cor,1}$ is the lateral strength of corroded columns at a given drift ratio θ (in percent) and $V_{u,1}$ is the lateral strength of identical uncorroded member.

CONCLUSIONS

This research focuses on validating a proposed approach to modelling reinforced concrete columns considering the proper extent of degradation in mechanical material properties due to loss of mass of corroded steel. After successful validation, the developed approach was used to conduct a parametric investigation of corroded columns with two main variables: the extent of corrosion (20% and 10%) and reinforcement detailing (anchored and lap splice). The major conclusion of this research is as follows:

1) Regression analysis of an updated database of 300 coupon tests of corroded steel was used to develop formulations for material properties of corroded steel (yield/ultimate strength and strain rupture).
2) A finite element modelling procedure was adapted and successfully validated taking corrosion damage into consideration. The procedure takes corrosion into consideration through the strength degradation in the following: (1) reinforcement yield strength; (2) reinforcement ultimate strength; (3) bar strain capacity; (4) bond stress-slip properties; (5) concrete cover strength.
3) From the parametric investigation, it is concluded that lap splice columns show higher damage in their corroded versions compared to columns with sufficient anchorage.
4) The strength reduction was 40% and 20% in the case of the lap splice and anchorage respectively, showing a more sever strength degradation in the lap splice case at the same level of corrosion.
5) The ultimate deformation capacity was significantly influenced by corrosion showing a reduction up to 45%.
6) Expressions for development of resistance curves for the sake of assessment were developed and provided in this research.

ACKNOWLEDGMENTS

The research presented here was funded through the Ontario Trillium Foundation and a Natural Sciences and Engineering Research Council of Canada-Discovery Grant.

REFERENCES

[1] ASCE/SEI 41. (2017). Seismic Evaluation and Retrofit of Existing Buildings. American Society of Civil Engineers.

[2] Fernandez I, Berrocal CG. Mechanical Properties of 30 Year-Old Naturally Corroded Steel Reinforcing Bars.(2019). *Int J Concr Struct Mater*, **13**(1):9.

[3] Tastani S, Pantazopoulou SJ. Recovery of seismic resistance in corrosion-damaged reinforced concrete through FRP jacketing. (2005). *Int J Mater Prod Technol*, **23**(3/4):389.

[4] Cervenka, V., Jendele, L., Cervenka, J. Theory. (2020). ATENA Program Documentation Part 1. Prague (Czech Republic): Cervenka Consulting.

[5] Goksu C, Ilki A. Seismic Behavior of Reinforced Concrete Columns with Corroded Deformed Reinforcing Bars. (2016). *ACI Struct J*, **113**(5):1053–64.

[6] El-Joukhadar N, Tsiotsias K, Pantazopoulou S. Consideration of the state of corrosion in seismic assessment of columns. (2019). *Int J Struct Integr*,**11**(2):239-247

[7] fib Model Code. Fib model code for concrete structures 2010. (2010). 436 p.

[8] Coronelli D, Gambarova P. Structural Assessment of Corroded Reinforced Concrete Beams: Modeling Guidelines. *J Struct Eng*. 2004 Aug 1; **130**(8):1214–24.

[9] Vecchio FJ, Collins MP. Modified Compression-Field Theory for Reinforced Concrete Elements Subjected to Shear. (1986). *J. ACI*, **83**(2):219–31.

[10] Menegotto, M., and Pinto, P. E. Method of Analysis for Cyclically Loaded Reinf. Concrete Plane Frames Including Changes in Geometry and Nonelastic Behavior of Elements under Combined Normal Force and Bending. (1973). *Proc.*, IABSE Symp. on Resistance & Ultimate Deformability of Structures Acted on by Repeated Loads, Lisbon.

[11] El-Joukhadar, N., Dameh, F. and Pantazopoulou, S.J. (2023). Seismic Modelling of Corroded Reinforced Concrete Columns, *Eng. Struct*. Vol (275).

[12] El-Joukhadar, N., S. J. Pantazopoulou and S. Pardalopoulos. The Role of Corrosion Damage in the Relevance of Seismic Assessment. (2020). Pap. # A02342, *Digital Proc.*, 17th WCEE, Sendai, Japan.